Received: 13 October 2020 | Revised: 19 March 2021 | Accepted: 21 March 2021

DOI: 10.1002/pc.26052

RESEARCH ARTICLE

spe INSPIRING PLASTICS PROFESSIONALS Polymer COMPOSITES WILEY

Comparative analyses of rice husk cellulose fiber and kaolin particulate reinforced thermoplastic cassava starch biocomposites using the solution casting technique

Benjamin Agyei-Tuffour[1,4] | Joshua Tuah Asante[1] | Emmanuel Nyankson[1] | David Dodoo-Arhin[1] | Michael Oteng-Peprah[2] | Salifu T. Azeko[3,4] | Ali Salifu Azeko[4] | Oluwaseun K. Oyewole[4] | Abu Yaya[1]

[1]Department of Materials Science and Engineering, School of Engineering Sciences, College of Basic and Applied Sciences, University of Ghana, Legon, Accra, Ghana

[2]Department of Water and Sanitation, University of Cape Coast, Cape Coast, Ghana

[3]Department of Mechanical Engineering, Tamale Technical University, Tamale, Ghana

[4]Department of Mechanical Engineering, Worcester Polytechnic Institute, Worcester, Massachusetts, USA

Correspondence
Benjamin Agyei-Tuffour, PhD, Department of Materials Science and Engineering University of Ghana, Legon, Accra, Ghana.
Email: bagyei-tuffour@ug.edu.gh

Funding information
University of Ghana BANGA-Africa Programme

Abstract

The potential of biodegradable packaging materials from thermoplastic cassava starch (TPS) reinforced with rice husk cellulose fibers (RHCF) and kaolin particulates (KP) using the solution casting method has been presented. This involved the blending of TPS and *RHCF/KP* in a plasticizer of ~4 ml of glycerol and ~45 ml of distilled water at 125°C and stirred at 60 rpm until a gel was formed. The gel was cast into sheets and bone-shaped tensile specimens and allowed to dry for 5 days and characterized. The results show a semicrystalline structure for TPS with an ~36% increase in crystallinity after reinforcement. The O-H bond stretching and the C-H bending bonds due to starch–glycerol reactions were the common functional groups in TPS–RHCF biocomposites, and Si-O-C bonds were characteristics of the silica phase in the kaolin. The water vapor transmission rate (WVTR) reduced to ~34% with KP reinforcements from ~238 g/m.day to 177 g/m.day and to ~74 g/m.day and ~164% for TPS–RHCF. The strength increased with up to 50 wt% kaolin content; ~0.96 MPa yield strength and ~2.60 MPa ultimate tensile strength (UTS) were recorded. For the RHCF reinforced composites, TPS-50 wt% also showed high strengths of ~0.96 MPa yield strength and ~3.50 MPa UTS. The WVTR reduced as content of kaolin was increased. Typically, from 0 to 30 wt% volume fraction of kaolin, the WVTR was reduced by ~34% to 177 g/m.day for TPS–kaolin and by ~164% to ~74 g/m.day in *TPS–RHCF*. The as-prepared biocomposites have potential as good packaging materials.

KEYWORDS

biocomposites, kaolin particulates, plasticizers, rice husk cellulose fibers, thermoplastic cassava starch (TPS)

1 | INTRODUCTION

Biodegradable plastic composites hold great promise as a reliable replacement for the nonbiodegradable petroleum plastics. Previous studies have reported on starch, chitosan, poly (lactic acid), polycaprolactone, and polyhydroxybutyrate as reliable biodegradable polymers according to.[1–3] Among the biodegradable polymers, starch is readily available at low cost and when reinforced, the limitations of starch bioplastics are

eliminated, resulting in a mechanically strengthened composite that can be used for packaging applications. Different types of fibers have been used as reinforcement in starch including natural fiber,[4] cellulose nanofibers,[5] rice and coffee husk cellulose fibers,[6] pulp microcellulose fibers,[7] sugar palm nanocellulose,[8] nanofibrillated cellulose[9] modified cellulose nanocrystals,[10] man-made fibers,[11] and particulate reinforcement.[12] In addition, thermoplastic cassava starch (TPS) has been reinforced with cellulose nanofibers from oil palm empty fruit bunches.[13] However, the authors are not aware of any studies and/or published articles in which cellulose fibers from rice husk produced from locally cultivated rice species and kaolin particles from Teleku Bokazo deposits in the western region of Ghana have been used as reinforcements in TPS biocomposite fabrication using the solution casting method.[14] This simple method has been reported to show good dispersion of the reinforcement in the polymer matrix. Again, the stepwise evaporation of the solvent has also been reported to influence the formation of 2D networks, which may affect the behavior of the composites physically, mechanically, and microstructurally.

Hence, in this paper, the analytical, numerical, and experimental results from the fabrication and characterization of starch bioplastics reinforced with rice husk cellulose fibers (RHCF) and kaolin particulates (KP) using the solution casting have been investigated. The properties of these bioplastic composites have therefore been compared, and their potential as packaging materials was evaluated. The TPS was reinforced with different volume fractions (0–50 wt.%) of RHCF and kaolin particles and characterized for their yield strength, tensile strength, and Young's modulus. Other analyses including Fourier transform infrared spectroscopy (FTIR), X-ray diffraction (XRD), scanning electron microscopy with energy-dispersive X-ray spectroscopy, water vapor transmission rate (WVTR), and thermal stability are presented. Finally, analytical and numerical modeling using the rule of mixture concepts, crack growth, and fracture toughness models to predict the stress distributions around the kaolin particles and the RHCF in the matrix of the TPS are presented and compared to assess the potential of the bioplastic composites for packaging applications.

2 | MATERIALS AND METHODS

2.1 | Raw materials processing

Kaolin lumps was obtained from Teleku Bokazo located in the Ellembelle district of the western region of Ghana (see Figure 1). The fine particle of the clay was achieved through continuous milling for about 10–15 h to obtain particle sizes of 120 μm–100 nm using a planetary ball mill, (PQ-N4 Mill; Across International, USA) operated at a frequency of 35 Hz for 5 h. Thermoplastic starch (TPS) with 100% chemical purity, yield of ~21.73%, amylose content of ~27.3%, and amylopectin of ~77.1% was acquired from Daejung Chemicals and Metals, Korea. The viscosity was ~3.229 ± 34 cP, and the pasting temperature was ~74.5°C. The TPS was used as the matrix in the fabrication of the biocomposites. The glycerol (propane 1,2,3-triol) with a purity of 99%, molecular weight of ~92.10, and refractive index of ~1.47 was obtained from Timstar Laboratory Suppliers Ltd., UK. NaOH, H_2SO_4, and HNO_3 were obtained from Sigma-Aldrich, UK.

The RHCF was extracted from the husk of locally cultivated rice species by grinding and sieving with an

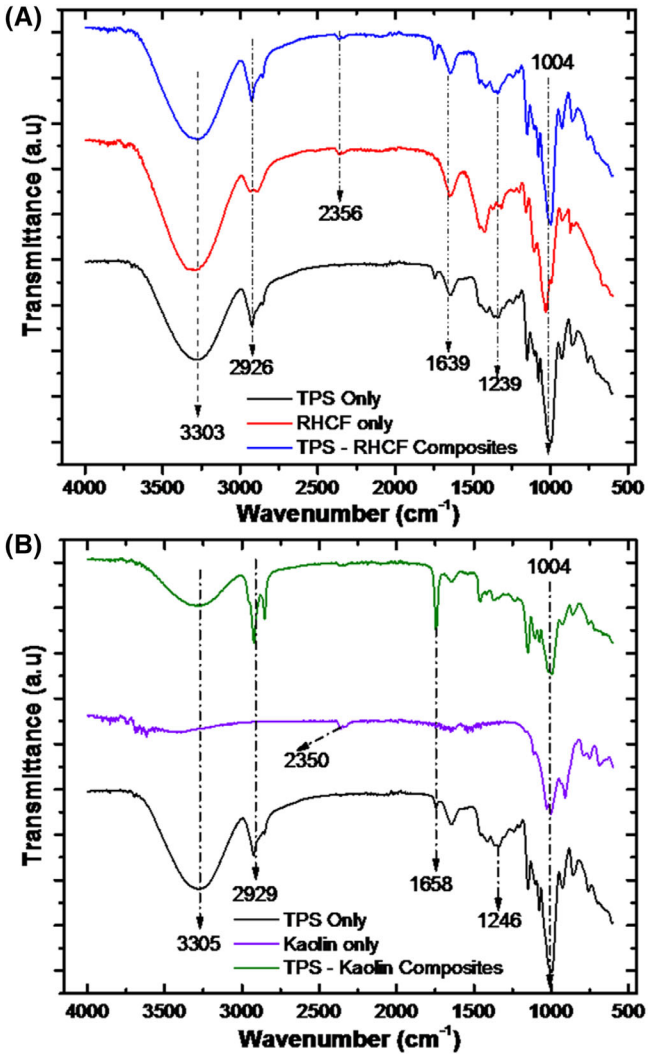

FIGURE 1 Fourier transform infrared spectra of (A) TPS–kaolin particulate and (B) TPS–rice husk cellulose fiber biocomposites

~120-μm sieve. The sieved material was treated with 1.0 M HNO_3 acid at room temperature under mechanical stirring for 24 h and washed with distilled water until the pH was ~5.0. Sodium hydroxide (1 M, NaOH) was added to the treated rice husk and stirred at room temperature for another 24 h. The solution was filtered using suction filtration. The procedure was repeated using a 6 M NaOH solution, and finally, a 4 M H_2SO_4 solution was added to the residue, stirred for 6 h, and filtered using a suction filtration method. The residue was then washed several times with distilled water until the pH was in the range of 5–6.

2.2 | TPS–RHCF and TPS–Kaolin biocomposites preparation

In the biocomposite preparation using the solution casting method, TPS is used as the matrix phase and RHCF/KP is used as the reinforcement. As a first step, ~ 4 ml of glycerol and ~45 ml of distilled water was used as plasticizers. The formulation of 10 g of TPS and 1.0 g of RHCF was added to the plasticizer, heated on a hotplate at 125°C, and stirred at 60 rpm until a gel was formed. The gel was then cast using bone-shaped molds and allowed to dry for 5 days. The same procedure was repeated for the different volume fractions of the RHCF and KP as shown in Table 1.

2.3 | Mechanical characterization of composites

The tensile specimen with gauge length of ~50 mm, width of ~20 mm, and a radius of curvature of ~5 mm was adopted in accordance with the ASTM standard D638M90 (Instron, 2020) using the Instron low-force mechanical tester (Instron, Canada). The ultimate tensile strength (UTS), elongation at break, modulus of elasticity, and yield and fracture strengths were determined. In all, eight samples were tested for each biocomposite formulation after drying at ~70 °C for 72 h and conditioning for 7 days in a relative humidity of ~60% according to[15].

2.4 | Water vapor transmission test

The water vapor transmission test was performed using the desiccator method according to ASTM E96 (ASTM E96-00, 2000)[16] with a specimen of ~3 mm dried at 70°C for 72 h. In this method, the weight of the sample attached to the beaker filled with water is taken before and after placing in the desiccator for 24 h. The weight loss of the sample attached to the beaker filled with water is calculated using Equation 1[13] to determine the WVTR value for each sample.

$$WVTR = \frac{W_s}{tA} \quad (1)$$

where "W_s" is the change weight of the specimen to be tested, "t" is the time at which the weight change occurs, and "A" is the area of the specimen.

TABLE 1 Batch formulation and volume fractions of thermoplastic cassava starch (TPS), kaolin, and rice husk cellulose fibers used in the biocomposites preparation

Sample (wt %)	Starch (g)	Cellulose fiber/kaolin reinforcements (g)
TPS only	10	0
TPS–10 wt% cellulose	10	1.0
TPS–20 wt% cellulose	10	1.9
TPS–30 wt% cellulose	10	2.9
TPS–40 wt% cellulose	10	3.9
TPS–50 wt% cellulose	10	4.9
TPS–10 wt% kaolin	10	1.0
TPS–20 wt% kaolin	10	1.9
TPS–30 wt% kaolin	10	2.9
TPS–40 wt% kaolin	10	3.9
TPS–50 wt% kaolin	10	4.9

2.5 | Microstructural and thermal analyses of composites

The surface morphology and chemical and mineralogical composition were studied in a scanning electron microscope coupled with an energy-dispersive X-ray spectrometer (Phenom ProX, Phenom World, the Netherlands) operated at ~15 kV using a tungsten filament. The nonconductive starch composites were initially sputtered with platinum (Pt) at 30 mA and 15 kV before the scanning electron microscopy (SEM) analyses.

The functional groups present in the biocomposite specimen were determined with the Bruker-Alpha Platinum-ATR machine (Bruker, France),[17,18] whereas the degree of crystallinity in the samples were determined using Bruker XE-T D2 phaser X-ray diffractometer (Bruker, France) equipped with a Cu-Kα anode radiation source operated at 30 kV and 10 mA. Samples were scanned within a 2Θ range from 5 to 65°.

The thermal stability, glass transition temperature, and the heat content of the cassava starch composites

were studied using Netzsch TG 209F1 (Netzsch Inc., MA, USA) thermogravimetric analyzer (thermogravimetric analysis [TGA]) and differential scanning calorimetry (DSC). The experiments were conducted in a nitrogen gas (N_2) atmosphere at a heating rate of 10°C/min from 25 to 900 °C.

2.6 | Finite element modeling of composites

The finite element modeling (FEM) was performed to further understand the interfacial interaction between the matrix and reinforcements using the ABAQUS™ package (Dassault Systemes Simulia Corporation, Providence, RI). Meshing was done using a four-node elemental mesh and ensured that fine meshes were used in the areas of matrix-reinforcement interfacial contacts. This is due to high stresses around such areas. To ensure stability of the simulations, the bottom boundary was fixed and uniform load was applied to the top. The stress distributions in the composite were estimated using the von Mises yielding criterion. The delamination of the fibers and particulates from the starch matrix were also modeled using interfacial fracture processes. The reinforcement and matrix with different elastic properties were assumed as presented in Table 2. Surface cracks were assumed to be present prior to the loading to measure the fracture toughness and the energy release rates (J-integrals) at the tips of the cracks between the matrix and reinforcements as reported by Oyewole et al.[19] and Asare et al.[20] in the expression presented in Equation 2:

$$G = f\left(\frac{-E_s}{-E_f}, \frac{t_s}{t_f}, \frac{d_b}{t_f}, \frac{d_t}{t_f}\right)\frac{\sigma^2 t_f}{-E_f} \quad (2)$$

where $\bar{E_f} = E_f/(1-\nu^2)$ and $\bar{E_m} = E_m/(1-\nu^2)$ are the plane strain elastic moduli of the reinforcement and matrix, respectively; d_t and d_b are the lengths of top and bottom interfacial cracks; and t_f and t_s are the thicknesses of the reinforcements and matrix, respectively. σ is the delamination stress.

TABLE 2 Mechanical properties of the materials used in the modeling of stress distribution in the biocomposites

Material	E (GPa)	Poisson ratio (ν)	Reference
Starch	2.7	0.4	[46, 47]
Kaolin	13	0.36	[48]
Cellulose fiber	12	0.30	[34, 49]

3 | RESULTS AND DISCUSSION

3.1 | Characterization of thermoplastic cassava starch, kaolin particulates, and rice husk cellulose fibers

Figure 1 presents the infrared spectra of the TPS cassava starch, TPS-RHCF and TPS-kaolin composites. FTIR peaks of TPS only can be found in Figures 1(A),(B). The figures show major bands at ~3287 cm^{-1}, ~2927 - ~2853 cm^{-1}, ~1656 cm^{-1}, ~1448–1345 cm^{-1}, and ~1003 cm^{-1} respectively in the TPS-only specimen. The OH stretching modes of water and glycerol in the TPS was reported at ~3287 cm^{-1} according to,[21,22] whereas the band at ~1656 cm^{-1} is mainly due to OH bending mode of water molecules used as a solvent in mixing the starch. The band at 2927–2853 cm^{-1} is due to the C-H stretching modes of the cassava starch–glycerol reaction and that between 1448 and 1345 cm^{-1} is due to the plane bending of the CH_2 molecules in starch. The band at ~1003 cm^{-1} is reported as C–O stretching modes in C-O-H and C-O-C in glucose ring.[23]

The main bands in the TPS–kaolin spectrum are shown in Figure 1(A) at ~3293 cm^{-1}, ~2932–2844 cm^{-1}, ~2363 cm^{-1}, ~1749–1640 cm^{-1}, ~1442–1376 cm^{-1}, ~1158–1004 cm^{-1}, and ~927–851 cm^{-1}. The bands are similar to those reported in the TPS only. However, the bands in the TPS–kaolin composites recorded higher intensity at ~2932 cm^{-1}.[24] The band at ~2363 cm^{-1} is also reported to be amide, which can be due to the introduction of nitrogenous compounds in the starch matrix during preparation. The bands at ~1749 cm^{-1} and ~ 1640 cm^{-1} are reported to be in-plane bending of C-H bonds in starch and the O-H bending mode in the water molecules, respectively. The C–O stretching normally of glucose ring was also reported at band ~1004–851 cm^{-1} and a new band at ~1158 cm^{-1}, which predicts the presence of Si–O–C bond due to the reaction between starch and the silicate phase.[24]

The bands recorded in the TPS–RHCF composites are presented in Figure 2(B) with the common bands at ~3287 cm^{-1}, ~2920 cm^{-1}, ~2352 cm^{-1}, ~1753–1646 cm^{-1}, ~1475–1195 cm^{-1}, and ~ 1000 cm^{-1}. Similar bands were recorded in the TPS at ~1000 cm^{-1}, represented the C–O stretching modes in C-O-H and C-O-C in glucose ring[25] because of the composition of the cellulose and the starch.

3.2 | Microstructure (SEM) elemental composition (EDX) and structural (XRD) analyses of biocomposites

Figures 2 and 3 show the SEM micrographs for the morphology of the TPS–kaolin (Figure 2) and TPS–RHCF

(Figure 3) composites taken at 10,000× magnification. The surface morphology of the TPS-only film in Figures 2 (A), 3(A) shows a relatively smooth and continuous layer-by-layer morphology, which confirms a dense and homogeneous structure.[26] However, there are patchy and rough cross-sections due to the flexible nature of starch in the network of starch–glycerol films.[27] The micrographs for TPS–kaolin biocomposites reported in Figure 2(A-F) show a good blend of the TPS and the kaolin. The Figure 2(A) is the pristine TPS with charged spots due to interaction with the electrons during the SEM analyses. Figure 2(B-F) is the images of 10 to 50 wt % kaolin reinforcement in TPS. From the microstructural images, it is noticed that the kaolin phases are uniformly distributed in the TPS matrix, resulting in relatively smooth morphology and improved texture. The SEM micrographs for TPS–RHCF biocomposites reported in Figure 3(A-F) indicate that the fibers were successfully

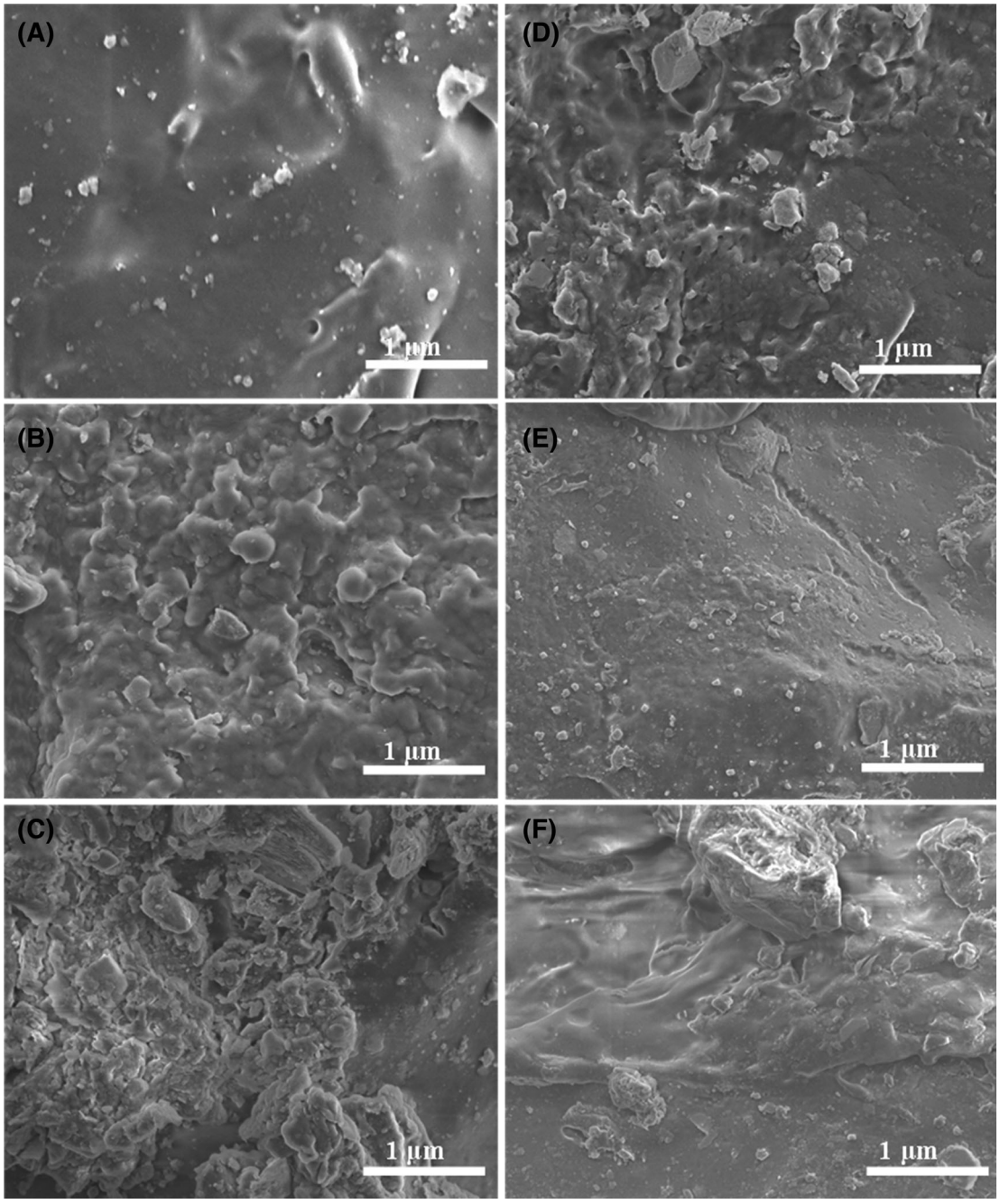

FIGURE 2 The microstructure and surface morphology of TPS–kaolin particulate composites: (A) TPS only, (B) TPS–10 wt% kaolin, (C) TPS–20 wt% kaolin, (D) TPS–30 wt% kaolin, (E) TPS–40 wt% kaolin, and (F) TPS–50 wt% kaolin. Images were taken at 10,000× magnification

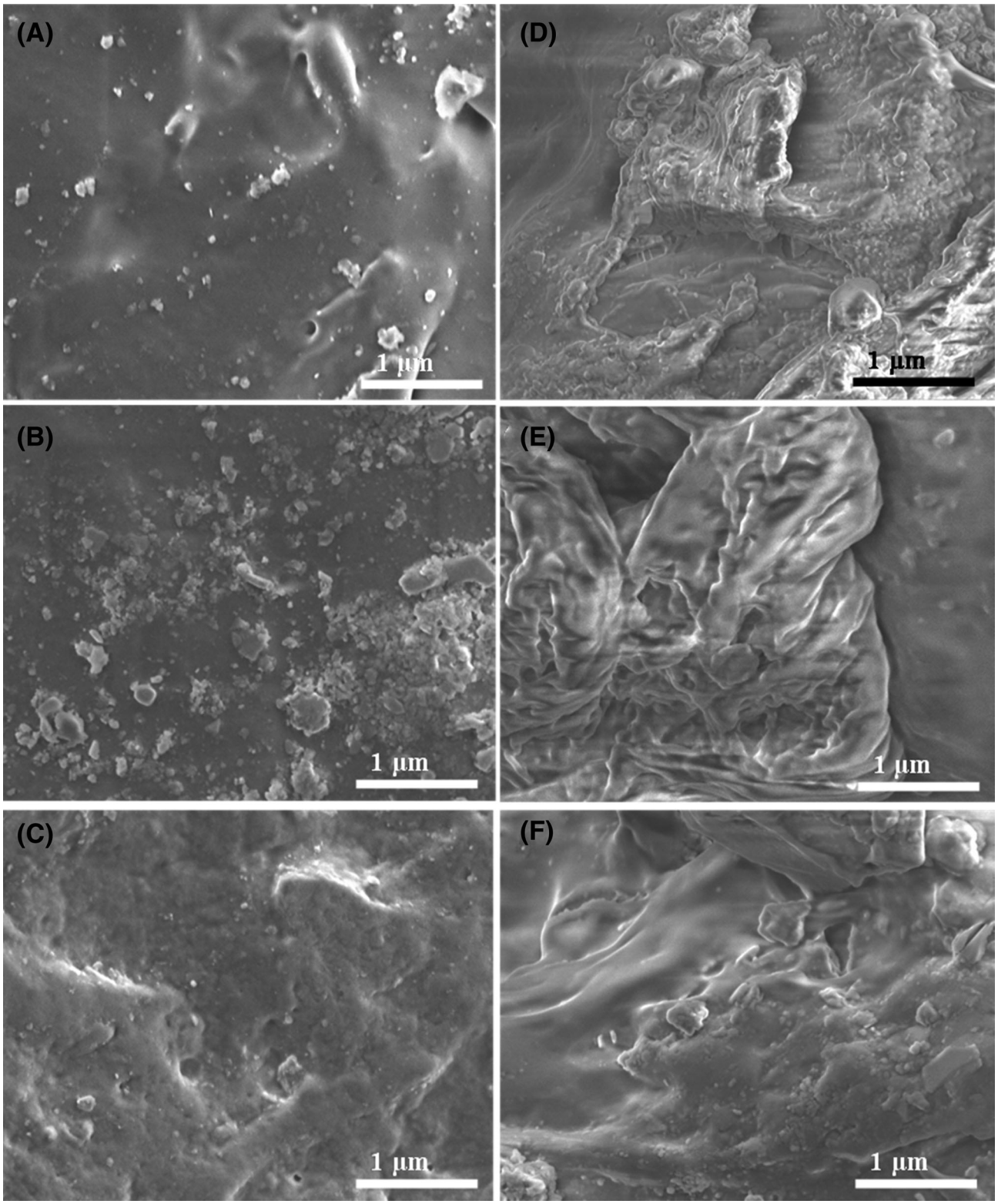

FIGURE 3 The microstructure and surface morphology of TPS–RHCF composites: (A) TPS only, (B) TPS–10 wt%, (C) TPS–20 wt%, (D) TPS–30 wt%, (E) TPS–40 wt%, and (F) TPS–50 wt% RHCF. Images presented were taken at 10,000× magnification

introduced into the TPS matrix, giving it a homogeneous morphology. Figure 3(B) however, has patches of cellulose fibers in irregular shapes, resulting in some agglomeration though the matrix generally looks homogeneous. The effects of the reinforcements in the composites are due to the interaction between the matrix and the

reinforcement as reported by[28]. It is interesting to note here that the common challenge of clay particle and fiber agglomerations, which often leads to weaker links in the composite and therefore compromises the mechanical behavior of the composites, is absent in this case.

In Figure 4, the X-ray diffraction (XRD) profiles and the elemental composition obtained from the EDX performed during the SEM analyses for TPS only (Figure 4(A)), RHCF–TPS composites (Figure 4(B)), and kaolin–TPS cassava starch composites (Figure 4(C)) are shown. The elements identified included C, Ca, O, Na, Si, and Al in their respective atomic weight percentages. C and O were the main elements found in the TPS only, whereas C, O, Si, and Al were found in the TPS–kaolin. This shows that the kaolin was successfully intercalated into the TPS matrix. The presence of Si, Al, and Ca in the RHCF–TPS cassava starch composites confirms that rice husk cellulose was used according to[30]. The presence of Na was a result of the sodium hydroxide used in extracting the cellulose fibers.

From the XRD results, the various representations of the peaks recorded on the diffractogram are indexed. Figure 4(D) shows the presence of three main crystalline minerals in kaolin. These minerals are kaolinite occurring at 12.5° and 24.5° (2 theta degrees), quartz occurring at 22.5° and 26.5° (2 theta degrees), and illite occurring at 7° and 27° (2 theta degrees). By comparing the peaks, it is evident that the intensities of the patterns for quartz and kaolin are dominant in the mineral than that of the illite phase. The reference

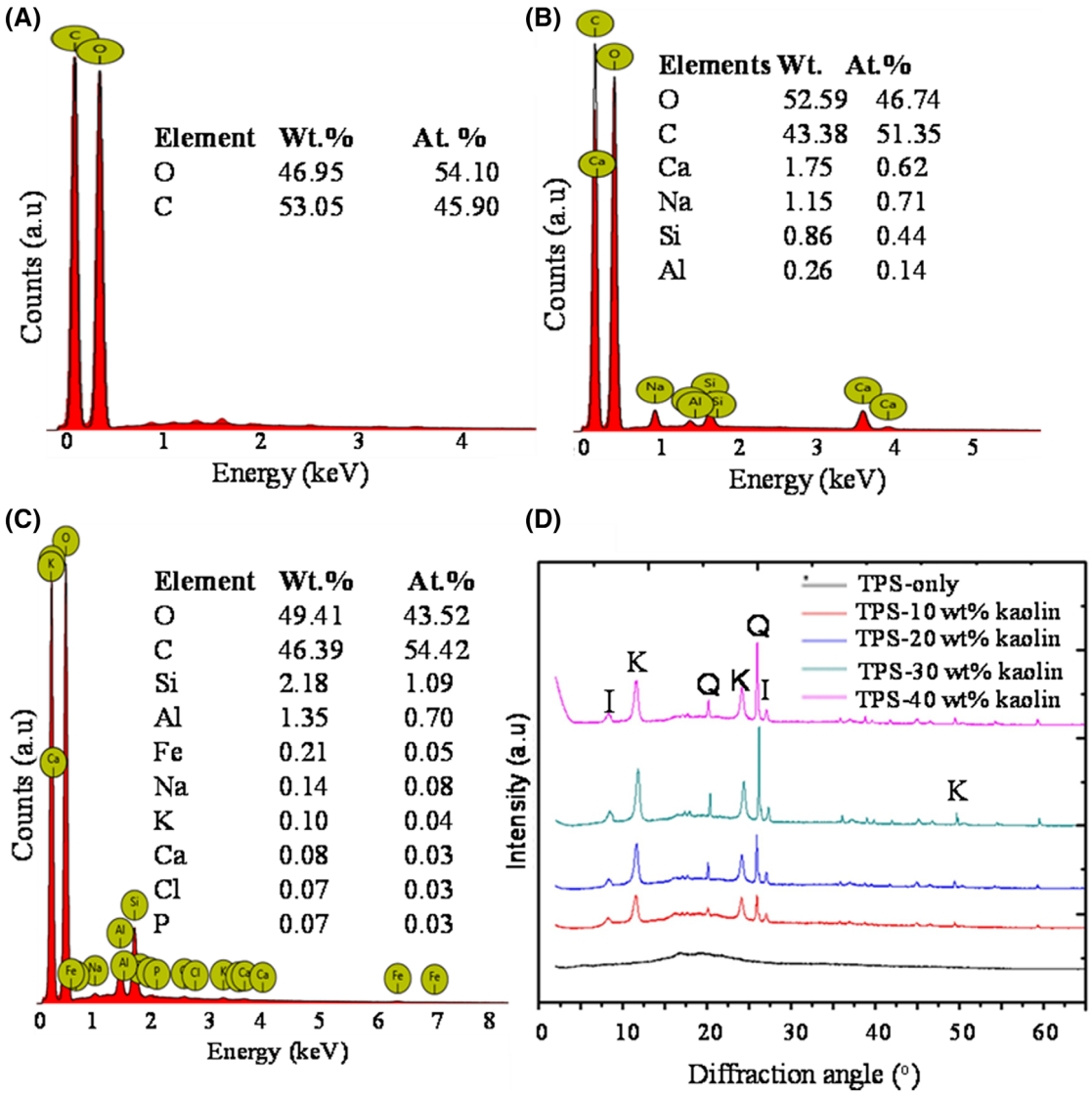

FIGURE 4 Energy-dispersive X-ray (EDX) and X-ray diffraction (XRD) spectra for (A) TPS only, (B) TPS–RHCF, (C) TPS–KP biocomposites, and (D) the peak intensities for the varying volume fraction of kaolin (0–50 wt%[29]

codes reported for the various mineral phases that are present in kaolin using X'Pert high score plus software include kaolinite (card no. 98-008-0082), quartz (card no. 01-087-2096), and illite (card no. 09-0334). It can be noticed that increasing the volume fraction of the kaolin results in an increase in the crystallinity of the composites and the subsequent effects on the mechanical properties. The higher the crystallinity of the composite, the stronger and brittle the composites become. The spectrum for TPS cassava starch only showed a semicrystalline material showing minor crystalline peaks at 2-theta values of ~16.4° and ~ 18.6° and the background depicting largely an amorphous material. The strong reflection at 16.4° is a characteristic of the starch type C known as polymorphic;[31] the peak at ~18.6° is of starch type A and B.[32]

3.3 | Mechanical characterization of biocomposites

3.3.1 | Stress–Strain curves

Typical stress–strain curves (Figure 5) and bar charts (Figure 6) are used to report the behavior of the composites when subjected to loading. The stress–strain curves using the Instron tensile tester on the TPS cassava starch–kaolin and TPS cassava starch–RHCF composites films are presented in Figure 5(A),(B) and Figure 6(A-D), respectively. From the curves and the charts, the yield strength, UTS, fracture strength, and Young's Modulus were determined. The yield strength of ~0.96 MPa and ~ 1.35 MPa were recorded for KP and RHCF reinforcements. Both reinforcements recorded average yield strengths of ~0.84 MPa and ~ 0.97 Mpa, respectively, and represented ~60% and ~125% increments as seen in Figure 6(A). It can also be seen that the yield strength increases with increasing volume fraction of the reinforcements. The tensile strengths recorded ~2.6 MPa and ~3.5 Mpa, respectively, with an average strength of ~1.6 MPa and ~2.15 MPa. These represent an increase of ~225% and ~ 337.5% in the strength upon reinforcement with KPs and RHCF and are presented in Figure 6(B). Young's modulus of ~116 MPa and ~80 MPa representing ~673% and ~433% were also recorded for the composites as shown Figure 6(C). The fracture strength also increased from ~0.8 to 1.58 MPa and ~2.1 MPa. The increments correspond to ~97.5 and ~140%, respectively. The yield strength shows the capacity of the composite to deform elastically prior to plastic deformation when subjected to loading in tensile mode, whereas the maximum strength of the composite before failure is the UTS similar to that presented by[33]. As the volume fraction of the kaolin is increased, the yield strength, UTS, and fracture strength increased. This was consistent with the prior studies by,[24,34] which stated that adding fillers with high aspect ratios such as nanokaolin and glass fiber increases the yield strength. However, the adhesion of the polymer and nanoclay interphase is compromised when the volume fraction of the nanoclay increases beyond ~30 wt%.

At these volume fractions the interaction of the RHCF and the starch polymer is seen to be very effective as seen in the SEM micrographs (Figures 2 and 3). They show uniform dispersion of the reinforcements in the

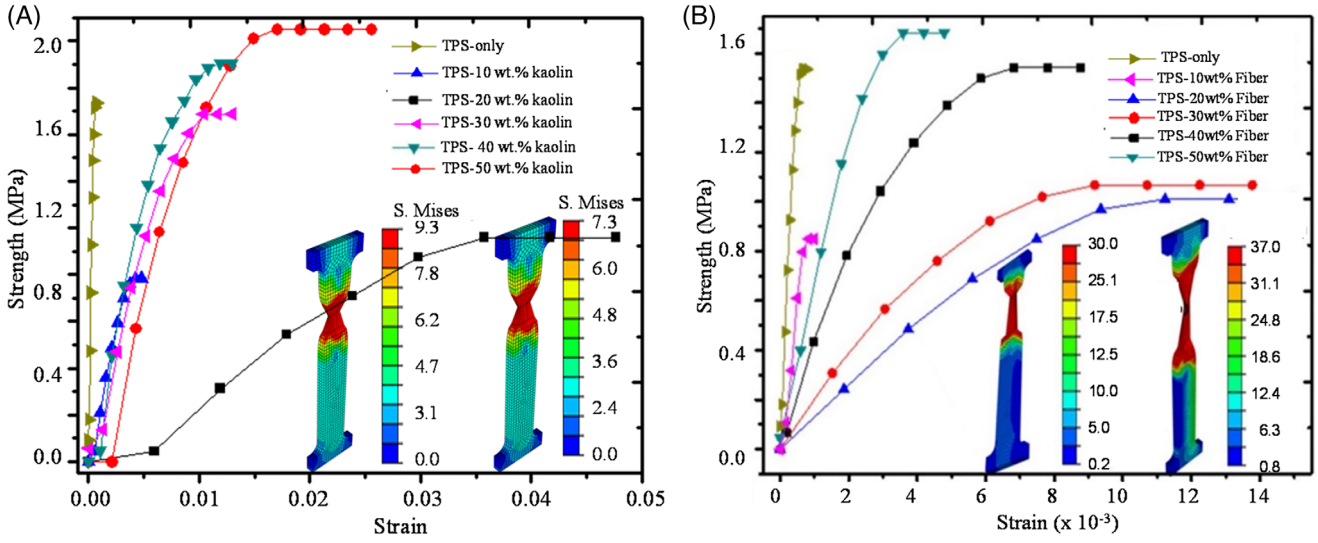

FIGURE 5 Stress–strain curves of (A) TPS–kaolin and (B) TPS–RHCF biocomposites. The inserts show the stress distribution in the two classes of biocomposites

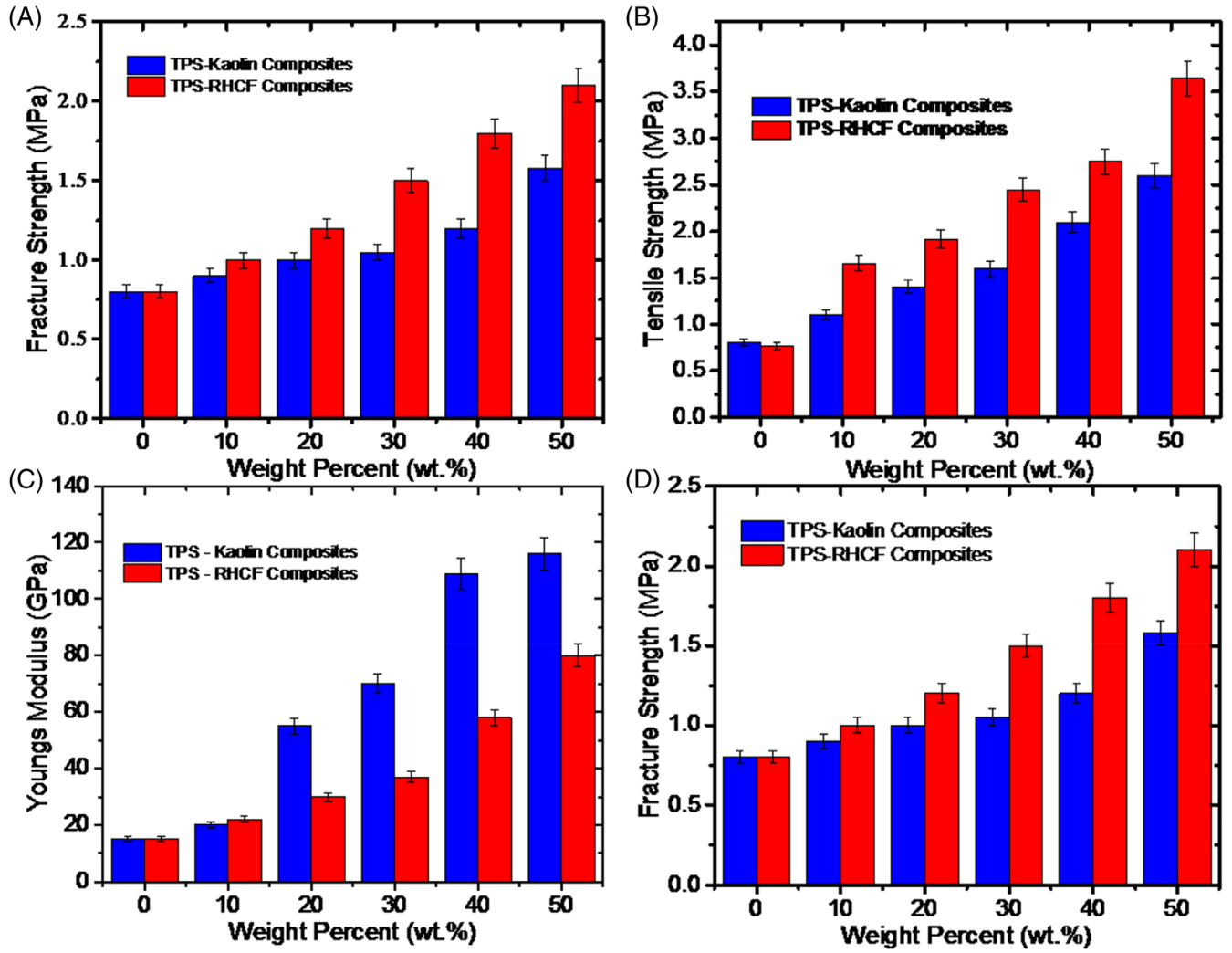

FIGURE 6 Mechanical properties of the biocomposites: (A) yield strength, (B) tensile strength, (C) Young's modulus, and (D) fracture strength of the TPS–kaolin particulate and TPS–rice husk cellulose fiber biocomposites

TPS matrices as reported by Matthew et al., (2014) for composites produced using solution casting. The improvement in the strength (fracture strength, yield strength, and UTS) is due to the wetting properties of the kaolin and the high aspect ratio of the RHCF used as modifiers in the biocomposite preparation. It can thus be deduced that when there is an improved interaction between the nanoclay–starch and RHCF–starch interfaces, the strength is improved.

3.4 | Water vapor permeability analyses of biocomposites

The water vapor permeability of the fabricated composites is shown in Figure 7 for TPS cassava starch–kaolin (Figure 7(A)) and the TPS–RHCF (Figure 7(B)). It can be seen that there is a reduction in the WVTR as the content of the clay increases from ~10 wt% to 30 wt%. Beyond the 30 wt%, there was a marginal increase in the transmission rate. This is because when the volume fraction of kaolin/nanokaolin increases in the sample, the crystallinity also increases; hence, the WVTR is improved.[35] However, with ~40 wt% kaolin, there is particle aggregation that leads to weaker interfaces between the starch and the kaolin/nanokaolin; hence, the water vapor goes through the spaces and voids created and results in high WVTR. A prior study by Agyei-Tuffour et al.[36] reported that kaolin particles have a high affinity for water and therefore could contribute greatly to the increase in the WVTR rates at higher kaolin/nanokaolin fractions.

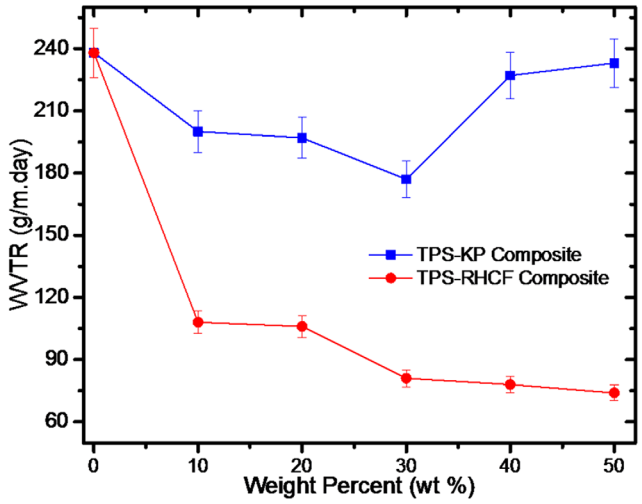

FIGURE 7 Water vapor transmission analyses of the biocomposites as a function of volume fraction of kaolin and rice husk cellulose fibers

Similar results are observed in the TPS–RHCF biocomposites, which show that increasing the volume fraction of RHCF decreases the WVTR rates. The TPS only is observed to have high WVTR, and considering the trend, it can be deduced that as the volume fraction of RHCF increases, the WVTR decreases. This is due to the hydrophilic nature of starch and the hygroscopic nature of the RHCF. As the RHCF increases, the starch content decreases and the dispersed phase of RHCF elongates the water particle portion. Hence, the biocomposite absorbs less water[37] due to the barrier created in the biocomposites when modified with RHCF in different volume fractions.

3.5 | Thermal stability analyses of biocomposites

Figure 8(A),(B) shows the thermographs for TPS–kaolin biocomposites and TPS–RHCF biocomposites, respectively. For kaolin-only thermographs, there is mass loss recorded in the temperature range of 450–600°C. The total mass loss observed for kaolin only was seen to be around 7.5%.

The thermograph of TPS–kaolin biocomposites shows four regions of mass loss.[38] The first one is between 60°C and 180°C corresponding to water loss, the second between 180°C and 240°C corresponding to evaporation of the glycerol, the third between 305°C and 358°C corresponding to starch decomposition, and finally a mass loss between 360°C and 600°C corresponding to the dehydroxylation of the silicates of kaolin.[39] The addition of kaolin into the starch matrix was seen to enhance the thermal stability of the composite. It was found that as the volume fraction of the kaolin increases from 0 to 50 wt%, the mass loss was reduced considerably. In the biocomposite, kaolin acts as a heat barrier, which improves the general thermal stability of the system.[40]

The thermographs for TPS–RHCF biocomposites show three regions.[41] The first region is between 60°C and 230°C corresponding to water loss and evaporation of glycerol, the second between 257°C and 370°C corresponding to the decomposition of starch, and the third region between 370°C and 665°C corresponding to the decomposition of RHCF structures.[42] It is noted that the biocomposite modified with 40 wt% volume fraction of RHCF is the most stable among the other TPS–RHCF biocomposites.

DSC was performed on the samples of mass ranges between 10 and 18 mg. The samples were heated from 10°C to 240°C at a heating rate of 5°C/min. The results for TPS–kaolin biocomposites and that for TPS–RHCF are shown in Figure 8(C),(D). As the volume fraction of kaolin is increased, the energy absorbed by the TPS–kaolin biocomposites is reduced to ~0.377 mW/mg for TPS–10 wt% kaolin biocomposite, ~0.335 mW/mg for TPS–30 wt% kaolin biocomposite, and ~0.323 mW/mg for TPS–50 wt% kaolin biocomposite. Similarly, it is noticed that as the volume fraction of cellulose fiber is increased, the endothermic peak is reached toward lower temperatures. A major change in the energy involved is also observed. For TPS only, the energy absorbed was ~0.399 mW/mg. For RHCF, the energy absorbed was ~0.711 mW/mg. As the volume fraction of RHCF is increased, the energy absorbed by the TPS–RHCF biocomposite is reduced to ~0.388 mW/mg for TPS–10 wt% RHCF biocomposite, ~0.378 mW/mg for TPS–30 wt% cellulose biocomposite, and ~0.357 mW/mg for TPS–50 wt% RHCF biocomposite.

3.6 | Analytical and Finite element analyses of biocomposites

3.6.1 | Analytical modeling of biocomposites

Figure 9(A-D) shows the results of the analytical modeling of the biocomposites using the rule of mixture concept as shown in Equations 3, 4 and 5. In Figure 9(A) the composite's modulus loaded in isostrain and isostress condition can be seen. The strength induced in the composites by the RHCF and KPs can also be seen in Figure 9(B) followed by the composites' fracture

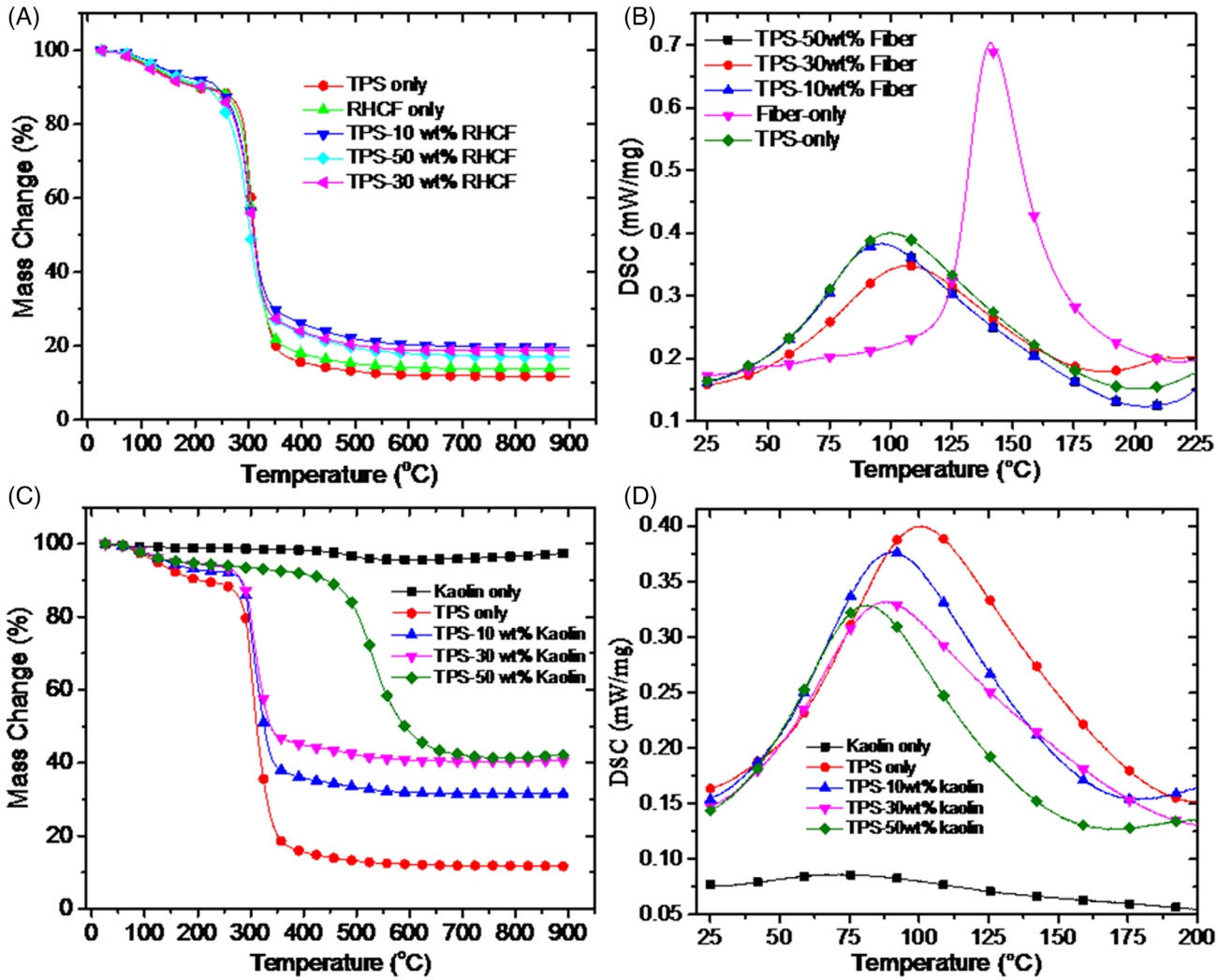

FIGURE 8 Thermal degradation rates (A-B) with the weight of samples (TGA) and the heat content analyses (DSC) of the biocomposites (C-D)

toughness (Figure 9(C)) and energy release rates at the TPS–RHCF interface (Figure 10(D)).

$$\sigma_c = \sigma_m V_m + \sigma_r V_r \tag{3}$$

$$E_c = E_m V_m + E_r V_r \tag{4}$$

and

$$E_c = \frac{E_m E_r}{E_r V_m + E_m V_r} \tag{5}$$

where the E_c, E_r, and E_m are Young's moduli of the composite, reinforcement, and matrix, respectively, whereasσ_c, σ_m, and $\sigma_r$are the strengths of composite, matrix, and reinforcement, respectively, with V_m and V_r as their volume fractions for isostrain and isostress conditions. It can clearly be seen that the composite moduli and yield strengths increased with increases in the volume fraction of the reinforcement. For example, a strength increase of ~4.5 MPa and ~5.2 Mpa, respectively, for TPS–RHCF and TPS–KPs compared with ~1.6 MPa for the TPS only at ~0.2 strain. This confirms that the TPS was uniformly reinforced with RHCF and kaolin particles. The effects of the reinforcements are seen in the formation of strong bonds between the components and the improved interface interactions between the TPS matrix and the fiber/kaolin particles. The fracture toughness as a function of the initial crack length before loading is shown in Figure 9(C), and the energy release rate between RHCF–TPS and TPS–kaolin interfaces is shown in Figure 9(D). It can be seen that the crack length increases up to a critical length (a_c), where the material's resistance to fracture is broken. Hence, the composite becomes susceptible to failure at this point and eventually to failure. From the results, the critical crack length

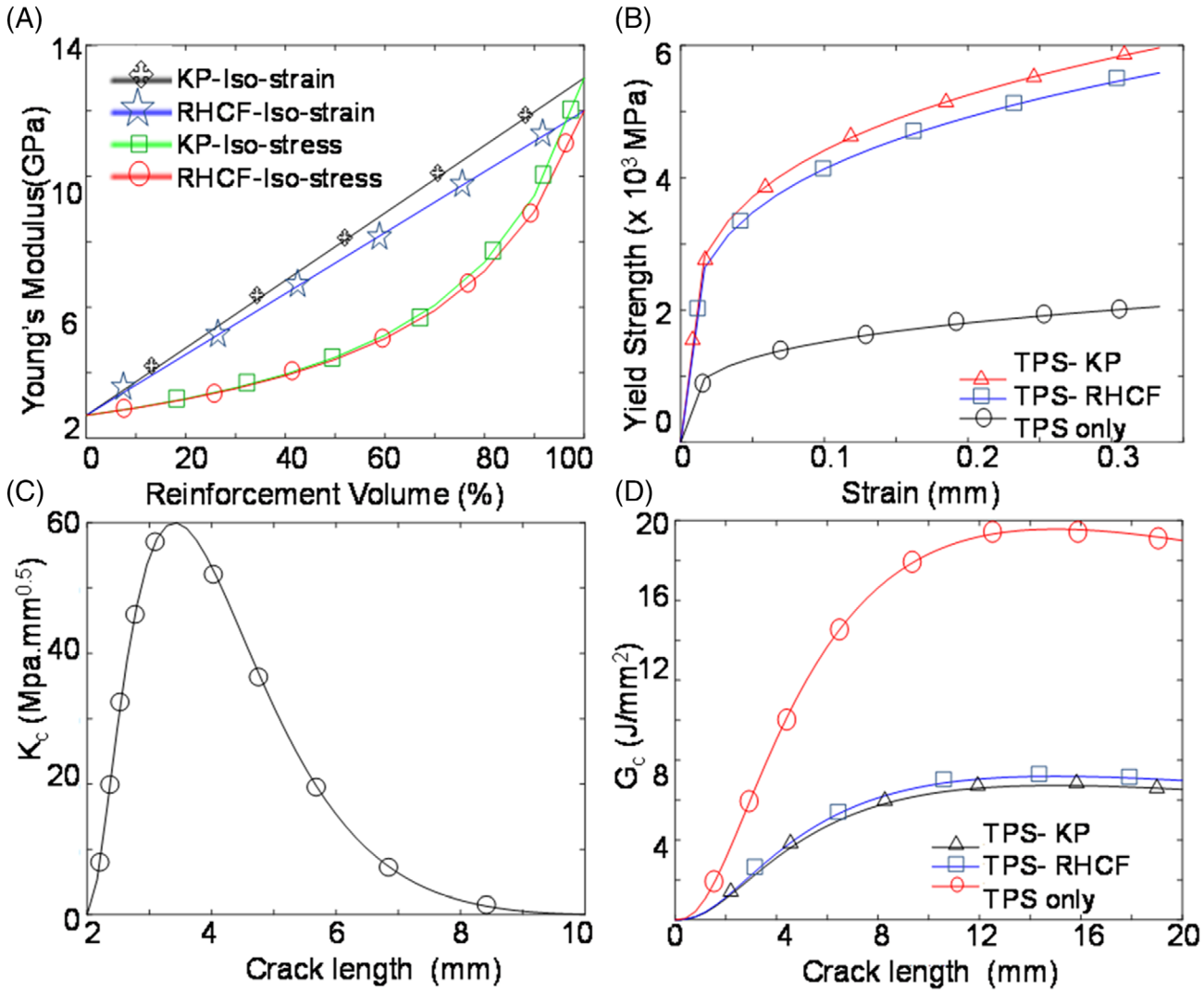

FIGURE 9 Analytical modeling of the composite deformation: (A) fracture toughness of TPS–cellulose fiber and (B) energy release rates (G_c) of TPS-only, TPS–RHCF, and TPS–kaolin biocomposites

beyond which the composite cannot resist fracture is ~3.4 mm.

Fracture toughness is the ability of a material to resist plastic deformation or fracture after a crack is developed. It is likened to the amount of energy released when an interface splits apart. This energy release rate is usually adopted in the analyses of fracture toughness in composites. Because fracture toughness is the resistance to fracture after a crack is developed, there must be enough energy available to overcome the resistance and allow the crack to propagate. From Equations 4 and 5, this energy represented with G must be at least equal to the critical energy (G_c) required to propagate the crack.[43]

$$G = G_c = R \tag{4}$$

$$K_{IC} = G = Gc = R = F\left(\frac{a}{w}\right)\sigma_f\sqrt{\pi a} \tag{5}$$

K_{IC} is the stress intensity (fracture toughness), $\sigma_f$is the flexural stress at the peak load, "a" is the crack length, and $F\left(\frac{a}{w}\right)$ is the compliance factor.

Similarly, because the fracture toughness is the composite's resistance to fracture failure when there is a crack, it provides useful insights into the behavior of biocomposites. There is crack propagation when the material is loaded. However, the material can transform the energy into breaking the intra- and interfiber/particle–starch bonds when it reaches the critical length. From Figure 10(B), the critical crack length where the material transforms the loading into breaking the bonds is

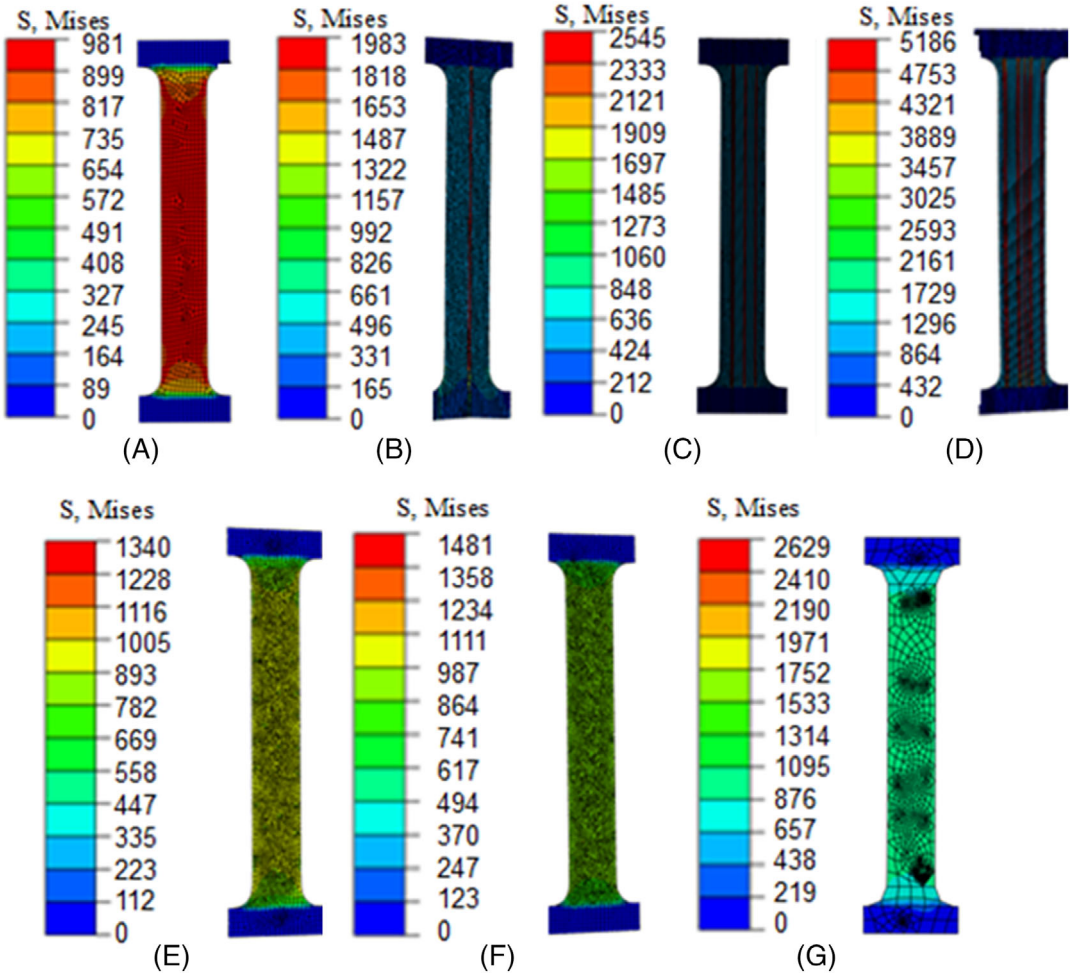

FIGURE 10 Finite element modeling of stress distribution in the composites: TPS only (A) and TPS–10 wt% (B), TPS–30 wt% (C), and TPS–50 wt% (D) TPS–RHCF. The TPS–kaolin biocomposites include TPS–10 wt% (E), TPS–30 wt% (F), and TPS–50 wt% (G)

~15 mm for TPS only and exceeds ~20 mm for RHCF and kaolin reinforced composites. Beyond this critical length, the composite cannot release the energy into breaking the bonds and that could lead to failure in the composite.

The associated energy release rates are ~1.95 J/mm^2, ~0.62 J/mm^2, and ~ 0.6 J/mm^2, respectively, for TPS-only, TPS–RHCF, and TPS-kaolin composites. This is due to the homogenous and compact nature of the TPS. With the addition of kaolin and RHCF, there is the creation of an interface, which is weaker in TPS–kaolin than in TPS–RHCF. As observed, the failure is related to the energy release rate in which recorded values for TPS–kaolin is lower compared with those for TPS–RHCF and TPS only. Therefore, TPS–kaolin composites will have greater fracture toughness than TPS–RHCF composites and TPS-only composites.

3.6.2 | Finite element analyses of composites

Using numerical modeling to further explain the mechanical behavior of the biocomposites, finite element analyses with Abaqus CAE software was used to model the mechanical response, and the results are presented in Figure 10(A-G). They show the von Mises stress distributions in the bone-shaped samples of TPS only (a), TPS–10 wt% (b), TPS–30 wt% (c), and TPS–50 wt% RHCF (d) and the stress distributions in the kaolin reinforced biocomposites for TPS–10 wt% (e), TPS–30 wt% (f), and TPS–50 wt% (g). These stress distributions depict the region in the composite with high-stress concentration and therefore give an indication of where failure can initiate in the composite. It can generally be seen that increasing the volume fraction of reinforcement leads to

an increase in the strength of the composite.[33,49–52] The TPS–RHCF composites recorded the maximum of ~51.86 MPa for TPS–50 wt% and ~1.98 MPa for TPS–10 wt%. The kaolin reinforced biocomposites recorded ~2.63 MPa for TPS–50 wt% and ~1.34 MPa for TPS–10 wt %, respectively. The TPS-only recorded the least strength of ~0.98 MPa. It can also be observed that the RHCF reinforced TPS composites show an enhanced strength compared with the kaolin reinforced biocomposites. This is largely due to the improved interaction between the fibers and the TPS and the weak interaction between the kaolin particles and the TPS. The fibers are continuously aligned, possess high longitudinal strength, and are compatible with the matrix unlike the KPs, which are rounded shapes, not continuous, and therefore have weaker intermittent joints throughout the composite. These results are in agreement with the experimentally determined mechanical properties and prior published works by.[33,49,50]

4 | CONCLUSIONS

TPS reinforced with RHCF and KPs have been investigated, and the results are compared in this paper. The FTIR analyses showed O-H bond stretching due to starch–glycerol reactions, O-H and C-H bending bonds as the common functional groups in TPS–RHCF biocomposites, whereas the Si-O-C bonds were a characteristic of the silica phase in the kaolin. The SEM analyses showed uniformly dispersed kaolin particles in the TPS–kaolin biocomposites. The crystallinity in the composites improved with the addition of reinforcements. For instance, at ~40 wt% kaolin volume fraction, the crystallinity increased from ~53.70% to ~90%. The TGA–DSC indicated loss in mass with temperature to assess the rate of degradation during disposal. Similarly, the WVTR reduced as content of kaolin was increased from 0 to 30 wt% from ~238 g/m.day to 177 g/m.day, an ~34% reduction. In the TPS–RHCF (0–50 wt%), the WVTR was reduced from ~238 g/m.day to ~74 g/m.day and ~164% reduction. The TPS-based composites recorded enhanced mechanical improvement. For example, the strength increased with up to 30 wt% kaolin content. Approximately 0.96 MPa yield strength, ~2.6 MPa UTS, and ~1.58 MPa fracture strength were recorded. For RHCF reinforced composites, the TPS–50 wt% RHCF sample also showed a high strength of ~0.96 MPa yield strength; ~3.5 MPa UTS and ~ 2.1 MPa fracture strength. It is therefore recommended that for the fabrication of TPS–kaolin composites, the volume fraction of the KPs should not exceed ~30 wt% and 50 wt% for the RHCF.

ACKNOWLEDGMENTS

The authors acknowledge support from the University of Ghana BANGA-Africa program. Grace Karikari Arkorful, Gloria Pokuaa Manu of the University of Ghana (UG), and Deborah Oyewole of Worcester Polytechnic Institute (WPI) are appreciated for their useful technical and laboratory assistance.

ORCID

Benjamin Agyei-Tuffour https://orcid.org/0000-0001-9629-8240

Abu Yaya https://orcid.org/0000-0001-6823-1276

REFERENCES

[1] T. Jiang, Q. Duan, J. Zhu, H. Liu, L. Yu, *Adv. Indus. Eng. Polym. Res.* **2020**, *3*(1), 8. https://doi.org/10.1016/j.aiepr.2019.11.003.

[2] A. Ashok, C. R. Rejeesh, R. Renith, *Int. J. Bio. & Biomats.* **2016**, *2*, 1.

[3] V. Siracusa, P. Rocculi, S. Romani, M. Dalla Rosa, *Trnd. Food Sci. Technol.* **2008**, *19*, 634. https://doi.org/10.1016/j.tifs.2008.07.003.

[4] J. Sahari, S. Sapuan, Z. N. Ismarrubie, M. Z. A. Rahman, *Fibr. Tex. East. Eur.* **2012**, *2*, 23.

[5] E. Pérez-Pacheco, J. C. Canto-Pinto, V. M. Moo-Huchin, I. A. Estrada-Mota, R. J. Estrada-León, L. Chel-Guerrero, *Intech Open Books* **2016**, *11*. https://doi.org/10.5772/65397.

[6] S. Collazo-Bigliardi, R. Ortega-Toro and A. C. Boix, *J. Renew. Mater*, **2018**, *6*(6), 599. https://doi.org/10.32604/JRM.2018.00127.

[7] N. Nordin, S. H. Othman, R. Kadir Basha, S. Abdul Rashid, *Food Res.* **2018**, *2*(6), 555. https://doi.org/10.26656/fr.2017.2(6).110.

[8] A. Nazrin, S. M. Sapuan, M. Y. M. Zuhri, *Polym.* **2020**, *12*, 2216. https://doi.org/10.3390/polym12102216.

[9] L. A. Granda, H. Oliver-Ortega, M. J. Fabra, Q. Tarrés, M. À. Pèlach, J. M. Lagarón, J. A. Méndez, *Polym.* **2020**, *12*, 1071. https://doi.org/10.3390/polym12051071.

[10] L. Huang, H. Xu, H. Zhao, M. Xu, M. Qi, T. Yi, S. An, X. Zhang, C. Li, C. Huang, S. Wang, Y. Liu, *New J. Chem.* **2019**. https://doi.org/10.1039/C9NJ02623A.

[11] S. Frackowiak, J. Ludwiczak, K. Leluk, *J. Polym. & Env.* **2018**. https://doi.org/10.1007/s10924-018-1301-9.

[12] Harunsyah, Sariadi, Raudah, *J. Phys: Conf. Ser.* **2018**, *953*, 012021. https://doi.org/10.1088/1742-6596/953/1/012021.

[13] F. Fahma, Sugiarto, T. C. Sunarti, S.M. Indriyani and N. Lisdayana, *Int. Jr. Polym. Sci.* **2017**, ID 2745721. https://doi.org/10.1155/2017/2745721.

[14] A. P. Mathew, K. Oksman, *Handbook of Green Materials* **2014**, 35. https://doi.org/10.1142/9789814566469_0018.

[15] J. Gironès, J. P. López, P. Mutjé, A. J. F. Carvalho, A. A. S. Curvelo, F. Vilaseca, **2012**, *72*(7), 858. ISSN 0266-3538. https://doi.org/10.1016/j.compscitech.2012.02.019.

[16] ASTM E96-00, 2000. www.astm.org. Accessed 13th December, **2020**.

[17] N. B. Colthup, L. H. Daly, S. E. Wiberly, *Introduction to infrared and Raman spectroscopy*, Academic Press, New York **1975**.

[18] P. R. Griffith, J. de Haseth, *A Fourier transform infrared spectroscopy*, Wiley, New York **1986**.

[19] O. K. Oyewole, D. Yu, J. Du, J. Asare, V. C. Anye, A. Fashina, M. G. Z. Kana, W. O. Soboyejo, *J. Appl. Phys* **2015**, *117*(23), 235501.
[20] J. Asare, S. A. Adeniji, O. K. Oyewole, B. Agyei-Tuffour, J. Du, E. Arthur, A. A. Fashina, M. G. Zebaze Kana, W. O. Soboyejo, *AIP Adv.* **2016**, 065125. https://doi.org/10.1063/1.4955141.
[21] J. Hong, X. A. Zeng, R. Buckow, Z. Han, M. Wang, *Food Hydrocolloids* **2016**, *54*, 139.
[22] M. Khalique, P. Ahmed, M. McLeod, J. Nézivar, W. A. Giuliani, *Spectroscopy* **2010**, *24*, 601. https://doi.org/10.3233/SPE-2010-0482.
[23] Y. Chen, X. Cao, P. R. Chang, M. A. Huneault, *Carbohydr. Polym.* **2008**, *73*, 8.
[24] N. Hassan, M. Mosadegh, *J. Polym. Environ.* **2011**, *19*, 980.
[25] G. Gündüz, O. Ali, Mehmet, *Wood. Cerne*. **2016**, *22*, 43. https://doi.org/10.1590/01047760201622012101.
[26] H. Dai, J. Yu, F. Geng, X. Ma, *Polym-Plast. Technol. Eng.* **2009**, *48*(8), 866. https://doi.org/10.1080/03602550902994938.
[27] Y. J. Liu, N. Xu, *Mech. Mats* **2000**, *32*, 769.
[28] K. K. Marfo, D. Dodoo-Arhin, B. Agyei-Tuffour, E. Nyankson, D. O. Obada, L. N. W. Damoah, E. Annan, A. Yaya, B. Onwona-Agyeman, M. Bediako, *Case Stud. Constr. Mats., Els* **2020**, *11*. https://doi.org/10.1016/j.cscm.2019.e00306.
[29] R. Suryana, Y. Iriani, F. Nurosyid, D. Fasquelle, *IOP Conf.: Mat. Sci. & Eng.*, **2018,** *367*(1), 012008.
[30] X. Ma, P. R. Chang, P. Zheng, J. Yu, *Carbohydr. Polym.* **2010**, *82*, 148.
[31] C. Mutungi, C. Onyango, T. Doert, S. Paasch, S. Thiele, S. Machill, D. Jaros, H. Rohm, *Food Hydrocolloids* **2011**, *25*, 477.
[32] M. Fazeli, R. Simao, *Plasma Process. Polym.* **2019**, *1*, e1800167. https://doi.org/10.1002/ppap.201800167.
[33] A. Pantano, B. Zuccarello, *Proc. Struct. Int.* **2018**, *8*, 517.
[34] C. DeArmitt, Functional fillers for plastics in *Applied Plastic Engineering Handbook*, William Andrew Publishing, Delmar, NY, USA, **2011**, p. 455. ISBN 9781437735147.
[35] Z. Duan & N. Thomas, *J. Appl. Phy.* **2014**, 115. https://doi.org/10.1063/1.4865168.
[36] B. Agyei-Tuffour, Y. D. Bensah, L. N. W. Damoah, D. Dodoo-Arhin, A. Yaya, E. Nyankson, E. Annan, E. Sarkodee, J. K. Efavi, *J. Polym. Comp* **2014**, *35*, 1507.
[37] N. R. Savadekar, V. S. Karande, N. Vigneshwaran, A. K. Bharimalla, S. T. Mhaske, *Int. J. Biol. Macromol.* **2012**, *2012*(51), 1008.
[38] A. Vázquez, V. Cyras, V. Alvarez, J. Morán, Jr. *Green Ener. and Techn*. **2012**, *50*, 287. https://doi.org/10.1007/978-1-4471-4108-2_11.
[39] M. Ashaduzzaman, D. Saha, R. M. Mohammad, *J. Compos. Sci* **2020**, *4*(2), 38. https://doi.org/10.3390/jcs4020038.
[40] V. P. Cyras, L. B. Manfredi, M. T. Ton-That, A. Vázquez, *Carbohydr. Polym*. **2007**, *106*(2), 749. https://doi.org/10.1016/j.carbpol.2007.11.014.
[41] T. Abbas, M. Rizwan, S. Ali, M. Adrees, M. Zia-ur-Rehman, M. F. Qayyum, Y. S. Ok, G. Murtaza, *Environ. Sci. Pollut. Res*. **2018**, *25*, 25668.
[42] N. Saba, A. S. Ismail, M. L. Sanyang, F. Mohammad, M. Pervaiz, M. Jawaid, O. Alothman, M. Sain, *Int. Jr. Biol. Macromol.* **2017**, *102*, 1. https://doi.org/10.1016/j.ijbiomac.2017.04.074.
[43] B. Lauke, *Polym. Lett* **2017**, *11*(7), 545.
[44] J. Schroeter, M. Hobelsberger, *Starch* **1992**, *44*(7), 247.
[45] Z. Zhou, Y. Zhang, X. Chen, M. Zhang, Z. Wang, *Int. Jnr. Food Sci.& Tech*. **2014**, *49*. https://doi.org/10.1111/ijfs.12593.
[46] N. H. Mondol, J. Jens, B. Knut, *The Leading Edge*, Soc. Expl. Geophys., OK, USA, **2008**, *27*(6), 1. https://doi.org/10.1190/1.2944161.
[47] R. Mao, N. Meng, W. Tu, T. Peijs, *Cellulose* **2017**, *24*, 4627. https://doi.org/10.1007/s10570-017-1453-0.
[48] R. J. Roberts, P. York, *Int. J. Pharm.* **1994**, *105*, 177.
[49] M. Alhijazi, Q. Zeeshan, Z. Qin, B. Safaei, M. Asmael, *Nanotechnol. Rev*. **2020**, *9*, 853. https://doi.org/10.1515/ntrev-2020-0069.
[50] Y. Glouia, Y. Chaabouni, A. El Oudiani, I. Maatoug, S. Msahli, *Int. J. Adv. Manuf. Technol*. **2019**, *103*, 4671. https://doi.org/10.1007/s00170-019-03838-4.
[51] D. Saravana Bavan, G. C. Mohan Kumar, **2013**, *Jr. Eng. 7*, 450381. https://doi.org/10.1155/2013/450381.
[52] L. José da Silva, T. H. Panzera, A. L. Christoforo, L. M. P. Durão, F. A. R. Lahr, *Int. J. Mater. Eng*. **2012**, *2*(4), 43. https://doi.org/10.5923/j.ijme.20120204.03.

How to cite this article: Agyei-Tuffour B, Asante JT, Nyankson E, et al. Comparative analyses of rice husk cellulose fiber and kaolin particulate reinforced thermoplastic cassava starch biocomposites using the solution casting technique. *Polymer Composites*. 2021;42:3216–3230. https://doi.org/10.1002/pc.26052